Chinese Journal of Chemical Engineering 53 (2023) 1–13

Contents lists available at ScienceDirect

Chinese Journal of Chemical Engineering

journal homepage: www.elsevier.com/locate/CJChE

Full Length Article

Exploring influence of MgO/CaO on crystallization characteristics to understand fluidity of synthetic coal slags

Meng Li [1], Jianliang Xu [1,*], Huixia Xiao [1], Xia Liu [1], Guangsuo Yu [1,2], Xueli Chen [1,*]

[1] Institute of Clean Coal Technology, East China University of Science and Technology, Shanghai 200237, China
[2] State Key Laboratory of High-Efficiency Utilization of Coal and Green Chemical Engineering, Ningxia University, Yinchuan 750021, China

ARTICLE INFO

Article history:
Received 3 October 2021
Received in revised form 9 March 2022
Accepted 14 March 2022
Available online 18 March 2022

Keywords:
Crystallization characteristics
Fluidity
Slags
MgO/CaO

ABSTRACT

The crystallization has significant influence on fluidity of slag and slag discharge of entrained-flow-bed (EFB) gasifier. The crystallization characteristics and fluidity of five synthetic slags with different MgO/CaO ratios prepared on the basis of the range of oxide contents of Zhundong coal ash were investigated in this study. The results show that with the MgO/CaO ratio increase, the initial crystallization temperature increases, and the main temperature range of crystallization ratio growth moves to higher temperature range gradually which causes T_{p25} (T_{p25} is the temperature corresponding to the viscosity of 25 Pa·s) to increase. Mg-rich crystals are formed preferentially than Ca-rich crystals when adding the same amount of MgO and CaO during cooling. The effective slagging operating temperature range decrease from 217 °C for the slag with a 0:4 MgO/CaO ratio to 44 °C for the slag with a 4:0 MgO/CaO ratio with the MgO/CaO ratio increase. The slags with 2:2 and 1:3 MgO/CaO ratios show similar effective slagging operating temperature range, T_{p25} and the temperature corresponding to the viscosity of 2 Pa·s. However, compared with the slag with a 1:3 MgO/CaO ratio, the crystallization ratio and rate of slag with a 2:2 MgO/CaO ratio are lower within lower temperature range (1300–1200 °C), causing its lower critical viscosity temperature and wider actual operating temperature range. Of the five slags, the widest effective slagging operating temperature range and the lowest T_{p25} of the slag with a 0:4 MgO/CaO ratio due to its low crystallization ratio, and wider actual operating temperature range of the slag with a 2:2 MgO/CaO ratio make the two slags suitable for slag discharge of EFB gasifier.

1. Introduction

An increasing demand for coal has become a considerable concern, making the effective utilization of coal crucial [1–3]. Gasification is an important technology that utilizes coal cleanly and efficiently [4–7]. Entrained-flow-bed (EFB) gasification technology is characterized by a wide range of raw materials, products with fewer impurities, and a high gasification intensity; consequently, it is one of the most widely used coal-conversion technology in the industry [8–10]. In the gasification process, a gasification agent reacts with coal and most of the organic matter in coal is converted into syngas at high temperatures (>1200 °C) [11–13]. The actual operating temperature of an EFB gasifier is maintained at approximately 50–200 °C above the flow temperature of coal to ensure that the inorganic matter in coal melts into molten slag, which is discharged from the EFB gasifier [14,15]. In addition, at the operating temperature, the viscosity of the slag is usually required to be lower than 25 Pa·s to avoid slag blockage [16]. The high gasification temperature makes the high temperature syngas and molten slag contain a lot of sensible heat when they exit the EFB gasifier. To recover the sensible heat and to remove the solid particles from the syngas, the EFB gasifier is usually equipped with a heat recovery system, such as a radiant syngas cooler and quench chamber. Some coal slag will crystallize in this system, leading to a sudden and great change in its rheological properties and a poor slag fluidity, which would in turn cause the slag to block the slag tap and affect the continuous operation of the EFB gasifier [16–19].

The chemical composition of coal ash has a significant effect on crystallization, thus affecting the fluidity of coal ash [20,21]. The acidic oxide, SiO_2, in coal ash is an important component of the network structure, while the basic oxides (Fe_2O_3, Na_2O, MgO, CaO, and K_2O) are oxygen donators aimed at destroying the network structure. The amphoteric oxide, Al_2O_3, shows different properties depending on the ratio of the basic to acid oxides of coal [22–25]. Ren *et al.* [26] found that with an increase in MgO content,

* Corresponding authors.
E-mail addresses: xujl@ecust.edu.cn (J. Xu), cxl@ecust.edu.cn (X. Chen).

https://doi.org/10.1016/j.cjche.2022.03.003
1004-9541/

the crystallization ability of the slag and the content of Mg-bearing minerals increased. The precipitation of Ca-bearing mineral could affect the crystalline phase content of the coal slag at high temperatures and the viscosity was closely associated with the crystalline phase content [27].

The influence of each oxide (CaO, MgO, Fe_2O_3, SiO_2, and Al_2O_3), the ratio of CaO/SiO_2 (binary basicity), the ratio of SiO_2/Al_2O_3, and the sum of $SiO_2 + Al_2O_3$ on the crystallization characteristics of coal slag have been widely investigated [19,26–30]. Both CaO and MgO are network modifiers [31,32]. The addition of MgO and CaO could lengthen the Si—O bond or release more free-ion bonds, to destroy the SiO_2 network structure [33]. Research has shown that the silicate structure would still change greatly when MgO replaced part of CaO in glass, in turn causing the crystallization behaviour and thermal properties of the glass to change [34,35]. Glass is considered similar with coal ash [36]. In recent years, the topic of using composite additives to improve the fluidity of coal ash has attracted extensive attention [37]. MgO and CaO are generally considered to contribute similar properties in regulating the ash fusion characteristics of coal. However, it was found that MgO and CaO exhibited synergy to reduce the ash fusion temperature (AFT) of coal, and a more significant fluxing effect was observed when MgO and CaO were added the same mass fraction rather than when used individually [38]. Jiang *et al.* [39] studied the effects of MgO/CaO ratios on the coal ash structure using molecular dynamics and thermodynamic calculation characterization at a microscopic scale. The results indicated that the effect of MgO on viscosity reduction was not apparent than that of CaO. However, when MgO replaced part of CaO in the binary SiO_2 ± CaO glass to become ternary system, the slag showed minimum viscosity [40]. Therefore, the influence of the relative contents of MgO and CaO on the viscosity of the slag is notably complex. The internal crystallization of the coal slag is an important factor affecting viscosity, and its mechanism of influence is not clear. Zhundong coal field is the second largest coal field in China. However, the MgO and CaO content of some Zhundong coals in the Xinjiang province is high, and the MgO content (2%–20%) fluctuates greatly in different mining areas. These Zhundong coals are high-alkali coals generally showing a low AFT suitable for the slag discharge in an EFB gasifier. However, its uncertain viscosity–temperature characteristics result in different slag discharge characteristics. Prior investigations cannot provide more comprehensive and accurate theoretical guidance for the Zhundong coal slag discharge. Research on the influence of MgO/CaO ratios on the crystallization characteristics and fluidity of coal slag are rare. Coal ash mainly contains oxides; however, it also contains some impurities. Synthetic slags, made from substitute materials, were often used in previous research to simplify the system [19,26–29]. Thus, in this study, the influence of MgO/CaO ratios on the crystallization characteristics was explored in order to understand the fluidity of synthetic coal slags and offer reference for improving the safety of slag discharge from Zhundong coal using an EFB gasifier.

2. Experimental

2.1. Synthetic slag samples

Synthetic slags were prepared by mixing seven pure oxides, as shown in Table 1. The synthetic slag contents, Al_2O_3, SiO_2, CaO, Fe_2O_3, Na_2CO_3, MgO, and K_2CO_3, were in the range of oxide contents found in common Zhundong coal ash in China. The contents of Al_2O_3, SiO_2, Fe_2O_3, Na_2O, and K_2O remained unchanged, and the total CaO and MgO content, being 23.86%, also remained unchanged. K_2O and Na_2O were replaced by K_2CO_3 and Na_2CO_3 through mass conversion calculations. The synthetic slags were divided into five groups by adjusting the ratio of CaO and MgO to retain the MgO/CaO mass ratio of 0:4, 1:3, 2:2, 3:1, and 4:0. Seven substitute materials were mixed until a homogenous state was achieved and then dried at 105 °C for 36 h. The five samples were then crushed to <200 μm.

2.2. Experimental methods

2.2.1. Water-quenched slag samples preparation

The five synthetic slags were melted, and water quenched in high temperature furnace under a reducing atmosphere (CO/CO_2 = 3/2, volume ratio). Put each slag into the crucible which could fill 1/2 of the volume of the crucible. The crucible was heated to 1200 °C at a heating rate of 20 °C·min^{-1}, then heated to 1500 °C at a heating rate of 10 °C·min^{-1} and then kept the 1500 °C with a following 30 min homoiothermal period. Finally, the slag was cooled to 800 °C at a cooling rate of 10 °C·min^{-1} and then quenched in ice water. The cooling rate of 10 °C·min^{-1} could avoid the problem of insufficient crystallization time caused by high cooling rate [28]. Remove the samples from the crucible and ground to less than 200 μm which were used for HTSM and XRD analysis.

2.2.2. XRD analysis

The mineral compositions of the sample slags were measured by X-ray diffraction (XRD) (PANalytical X'Pert Pro PW 3040, The Netherlands) with Cu K_α radiation, which were operated with 40 kV and 40 mA, and the scanning was from 2θ = 10°–70° with 0.01° step size.

2.2.3. Thermodynamic calculation

FactSage software contained a series of calculation modules through which various thermochemical data could be obtained [41,42]. The theoretical crystalline phase compositions and the Gibbs free energy (ΔG) of solid and liquid phases were calculated by the equilib module of FactSage 7.2 during cooling process. The ΔG were calculated according to the formula ($\Delta G_{solid}=\Delta G_{total} - \Delta G_{gas} - \Delta G_{slag}$). The operations were conducted from 1500 to 800 °C under reducing atmosphere (3:2, CO/CO_2, volume ratio) with a 50 °C interval.

2.2.4. In situ experimental method

Experiments on slag cooling of five samples were conducted on the HTSM system which was mainly composed of two parts: a high temperature stage (Linkam, UK) and a microscope (DM4500P Leica, Germany) [43,44]. The operation steps were as follows: the samples were put on a sapphire slip and heated up to 1500 °C according to the heating procedure of water quenching experiment and kept for 10 min to make them melt fully. Finally, cool down the samples at a cooling rate of 10 °C·min^{-1}. The surface morphology of the slag at different temperatures was photographed during the cooling process on the HTSM. The shooting temperatures were as follows: the maximum temperature of HTSM heating to ensure full melting (1500 °C), the temperature at an interval of 100 °C after the maximum temperature under cooling process, the initial crystallization temperature, the final crystallization temperature, and the temperatures 50 °C lower than the final crystallization temperature which determined the final crystallization temperature. ImageJ software was used to analysis crystallization ratio during cooling process. Finally, the samples were taken out from HTSM and used for SEM-EDS analysis.

2.2.5. SEM-EDS analysis

The magnification of HTSM system could not meet the experimental requirements, the samples from HTSM were gilded and crystal morphology was observed by SU-1510 scanning electron

Table 1
Chemical composition of the five synthetic slags with different MgO/CaO ratios

Composition/% (mass)	MgO/CaO (0:4)	MgO/CaO (1:3)	MgO/CaO (2:2)	MgO/CaO (3:1)	MgO/CaO (4:0)
SiO_2	40.51	40.51	40.51	40.51	40.51
Al_2O_3	16.27	16.27	16.27	16.27	16.27
Fe_2O_3	17.02	17.02	17.02	17.02	17.02
CaO	23.86	17.90	11.93	5.97	0.00
MgO	0.00	5.97	11.93	17.90	23.86
Na_2O	1.54	1.54	1.54	1.54	1.54
K_2O	0.80	0.80	0.80	0.80	0.80

microscope (Hitachi, Japan) and local element compositions of them were detected by an energy dispersive spectrum system (EDAX, America).

2.2.6. Slag viscosity measurement

The viscosity of the synthetic slags was measured using a RV DVIII high temperature rotational viscometer (Theta, America) based on the Chinese Standard GB/T 31424—2015. The synthetic slag was first pre-melted, and thereafter 40 g of the pre-melted slag was placed in the corundum crucible. The corundum crucible was fixed with a corundum bracket in the furnace, and the whole system was vacuumized by a vacuum pump. A gas mixture (CO_2: CO = 2/3, volumetric) was then injected into the system to ensure that the test was performed in a weak reducing atmosphere. The system was heated to 1550 °C. The spindle was lowered in a controlled manner until it was immersed in the slag, and the viscosity value was recorded by a viscometer at intervals of 5 s.

3. Results and Discussion

3.1. Crystalline phases transformation

The samples were heated to 1500 °C and were fully melted. Thereafter, the slag was cooled to 800 °C at a cooling rate of 10 °C·min^{-1} and quenched in ice water. The final crystalline phase of the water-quenched slag samples could be analysed by XRD. Fig. 1 shows the XRD patterns of slag with different MgO/CaO mass ratios. Weak anorthite ($CaAl_2Si_2O_8$) diffraction peaks are detected for the synthetic slag with a 0:4 MgO/CaO mass ratio. As the MgO/CaO ratio increase to 1:3, the anorthite diffraction peak intensity increase noticeably and a diopside ($CaMgSi_2O_6$) diffraction peak appears. The addition of Ca^{2+} and Mg^{2+} combined with O^{2-} result in a decrease in Si—O and Al—O, which causes the number of non-bridged oxygen bonds to increase and that of bridged oxygen bonds to decrease in the slag [22,26,45]. The network structure is destroyed, and the degree of ions freedom increase, which promote the crystallization of slag [46,47]. When the MgO/CaO ratio increase to 2:2, the diffraction peak intensities for both the anorthite and diopside decrease. In addition, a noticeable forsterite (Mg_2SiO_4) diffraction peak appears. When MgO/CaO increase to 3:1, the dominant crystalline phase of the slag change from Ca- to Mg-bearing minerals and no obvious diopside diffraction peak is observed. It is speculated that the addition of MgO can promote diopside formation. However, it was beneficial to the formation of diopside with the higher content of CaO and lower content of MgO. An increase MgO/CaO ratio cause more Mg^{2+} to enter the spinel and olivine. When the ratio of MgO/CaO is 4:0, Ca-bearing minerals disappear. The crystalline phase is mainly composed of forsterite (Mg_2SiO_4), ringwoodite (Fe-rich $(Mg,Fe)_2SiO_4$), spinel (Fe-rich (Mg (Fe,Al) $_2O_4$)), and hercynite ($FeAl_2O_4$).

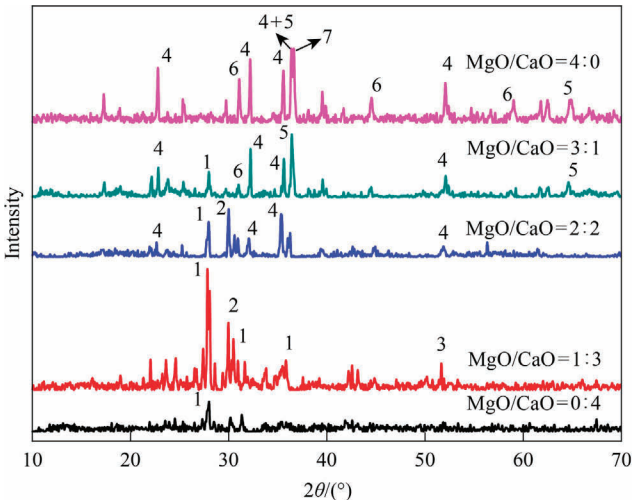

Fig. 1. XRD patterns of the synthetic slags with different MgO/CaO ratios (1. anorthite ($CaAl_2Si_2O_8$); 2. diopside ($CaMgSi_2O_6$); 3. hedenbergite ($CaFeSi_2O_6$); 4. forsterite (Mg_2SiO_4); 5. spinel Fe-rich (Mg (Fe, Al)$_2O_4$); 6. hercynite ($FeAl_2O_4$); 7. ringwoodite, Fe-rich ((Mg, Fe)$_2SiO_4$)).

3.2. Simulation of theoretical minerals using FactSage software

FactSage software simulated the change in theoretical mineral compositions and relative liquid phases of the slag during the cooling process based on the ash composition, thus deducing the evolutionary process of the crystalline phase. Fig. 2 shows the change in crystalline phase composition and relative liquid phase of the five samples. In comparison, the liquid phase content gradually decreases with the decrease in temperature, and the initial temperature of crystalline phase increases with the MgO/CaO ratio increase. As shown in Fig. 2(a), when the MgO/CaO ratio is 0:4 (*i.e.* no MgO addition), the temperature range for the growth of Ca-bearing minerals is 1250–1000 °C and the minerals are predominantly anorthite, melilite, and diopside ($CaAlSi_2O_6$). Fig. 2(b) shows that when the MgO/CaO ratio is 1:3, anorthite and olivine precipitate preferentially from molten slag, and thereafter melilite and diopside ($CaMgSi_2O_6$ and $CaAlSi_2O_6$) appear with the decrease in temperature. The anorthite, olivine, and melilite transform into diopside at a low temperature range, and the crystalline phase is composed predominantly of diopside in the final crystalline phase. However, the synthetic slag still shows a high anorthite diffraction peak in the XRD spectrum, as shown in Fig. 1. This may be due to the high viscosity within the low temperature range, which hinders the transmission of protons and energy. This result in a serious limitation of the transformation and growth of crystals; hence, a large number of minerals in the slag still exist in the form of anorthite. As shown in Fig. 2(c), when the MgO/CaO ratio is 2:2, the initial crystallization temperature of Mg-bearing minerals is higher than that of Ca-bearing minerals. In addition, the relative content of anorthite and diopside decrease, while that of Mg-bearing spinel and Mg-bearing olivine increase. As shown in

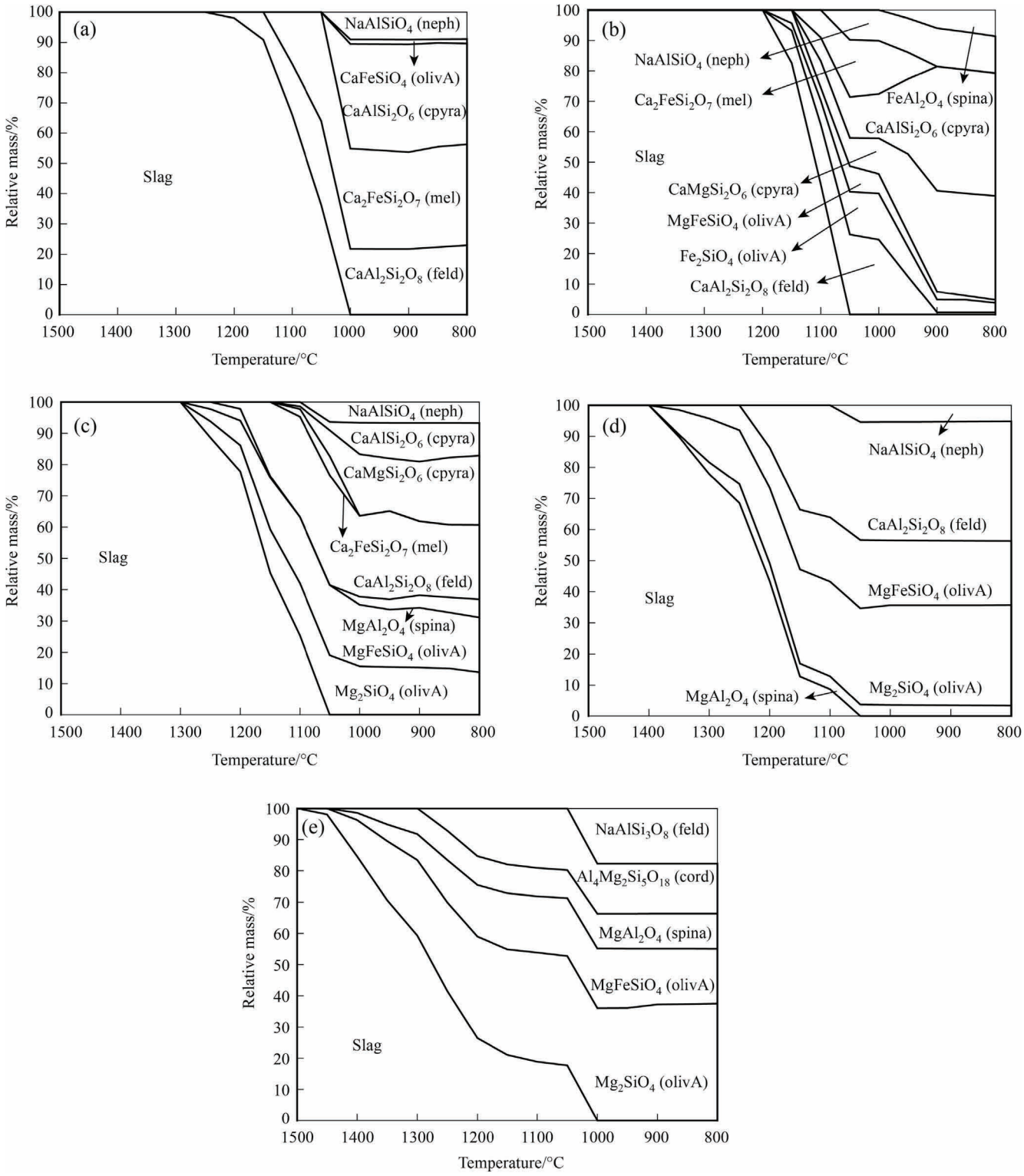

Fig. 2. Theoretical mineral compositions of the synthetic slags with different MgO/CaO ratios: (a) MgO/CaO = 0:4; (b) MgO/CaO = 1:3; (c) MgO/CaO = 2:2; (d) MgO/CaO = 3:1; (e) MgO/CaO = 4:0.

Fig. 2(d), when the MgO/CaO ratio is 3:1, the relative content of Mg-bearing minerals is higher than that of Ca-bearing minerals and the diopside disappear. These results are consistent with the XRD results. As shown in Fig. 2(e), when the MgO/CaO ratio is 4:0, the Ca-bearing minerals disappear, the crystal growth of Mg-bearing minerals is in the higher temperature range, and the content of Mg-bearing minerals does not change when the temperature is below 1200 °C. From the above analysis, it is speculated that Ca-bearing minerals are harder to crystallize than some Mg-bearing minerals at higher temperatures, and the addition of MgO endows the crystallization with a more perceptible enhanced tendency than that of CaO [33]. This may be possibly related to the longer equilibrium interatomic distance of Ca—O (0.23 nm) than that of Mg—O (0.195 nm), indicating that the binding ability of

Mg and O is stronger than that of Ca [20,31,48]. The main XRD minerals, *i.e.* anorthite, diopside, the spinel containing Fe and Mg, and the olivine containing Fe and Mg, as shown in Fig. 1 show the same trend as seen *via* FactSage with an increase MgO/CaO ratio. However, numerous theoretical crystalline phases appear in the FactSage analysis, while only some main minerals are detected in XRD. It may be that FactSage calculate the crystallization process in a complete equilibrium state, in which the crystallization time is sufficient, and the hindrance of the proton and energy transmission is not considered. In contrast, the experiment is dynamic and cannot reach a completely equilibrium state; therefore, the experimental conditions may not meet the precipitation and growth conditions of some crystalline phases, such as melilite and clinopyroxene [19]. An alternative cause may be a difficulty in marking the diffraction peaks of some crystals, which are in the form of dispersion peaks in the XRD pattern, due to their small content in the crystalline phase, the fine grains, and high disorder [15].

3.3. Simulation of ΔG changes using FactSage software

Fig. 3 shows the changes in ΔG calculated by FactSage with different MgO/CaO ratios during the slag cooling process. The ΔG of the liquid phase presents a tendency to increase with decreasing temperature, which indicates that the liquid phase formation trend decreases, and the stability of the liquid phase system decline. The ΔG of the solid phase has the opposite effect to that of the liquid phase, and the ΔG decreases with decreasing temperature, which indicates that the solid phase formation trend gradually increases, and the solid phase system became more stable. In comparison with the theoretical mineral results, as shown in Fig. 2, it can be concluded that the crystalline phasebegins to precipitate when the ΔG value of the liquid and solid phases start changing noticeably. As the temperatures continue to decrease, finally, the ΔG of the liquid and solid phases do not noticeably change and the total crystalline phase content do not change; however, the transformation between the crystalline phases may have continued. As shown in Fig. 3, when the MgO/CaO ratio is 1:3, the ΔG of the solid phase shows a slight change when the ΔG of the liquid and solid phases tend to stabilise in the lower temperature range, resulting potentially from the transformation of numerous crystalline phases into diopside in the lower temperature range of Fig. 2(b). Thus, there is a strong diopside diffraction peak for the slag with a 1:3 MgO/CaO ratio in the XRD diagram shown in Fig. 1. With an increase MgO/CaO ratio, both temperatures, at which the ΔG of two phases begin to change and stop changing obviously increase gradually. This indicates that the initial crystallization temperature increases, and the crystallization temperature range moves towards a higher temperature range with an increase in the MgO/CaO ratio.

3.4. In situ observation of HTSM

HTSM observed the crystal precipitation, phase distribution, and morphology of the slag surface during the cooling process. Figs. 4–8 show the crystalline phase changes of the five samples with MgO/CaO ratios of 0:4, 1:3, 2:2, 3:1, and 4:0 in the temperature range (1500–800 °C) at cooling rate of 10 °C·min^{-1}. As shown in Fig. 4, a small amount of flaky mineral appears at 1260 °C when the MgO/CaO ratio is 0:4. The crystals are formed gradually with decreasing temperature. There is little difference in the surface morphology at 1100 and 1050 °C, indicating that the crystal growth was complete at 1100 °C. In addition, it is observed that smooth glassy minerals accounting for a large portion and the slag shows a trend of continuous condensation and volume of that shrunk. As shown in Fig. 5, when the MgO/CaO ratio increases to 1:3, the initial crystallization temperature increase and thinner crystals shaped as long bars, needles, and sheets are formed. As the temperature decreases, the crystals gradually became thicker and larger, and the crystal growth was complete at 1100 °C. At this time, it is clearly that the slag is almost entirely crystalline, and no obvious smooth glassy substancesare observed. As shown in Fig. 6, when the MgO/CaO ratio is 2:2, small size crystals are precipitated preferentially at 1450 °C and the acicular crystals appear at 1400 °C thereafter, while some smooth glassy minerals are still observed when crystallization is complete. As shown in Fig. 7, when the MgO/CaO ratio is 3:1, small size crystals appear at 1450 °C and the small size crystal content increases with decreasing temperature. Most of the small size crystals are linked into a network. However, the smooth glassy substance still accounts for a large proportion when the final crystalline phase is reached (1100 °C). Fig. 8 shows that when the MgO/CaO ratio is 4:0, small size crystals appear at 1475 °C and the crystalline phase content increases rapidly with decreasing temperature. The dense small size crystals were observed when the crystalline phase stops changing (1200 °C), and the proportion of the glass phase is very low. The crystallization temperature range is the highest when CaO is not present and only MgO exist. This is consistent with the crystallization temperature range calculated by FactSage, as shown in Figs. 2(e) and 3(e). When comparing the changes in the crystalline and glass phases of the five samples upon the completion of crystallization, it can be concluded that with an increasing MgO/CaO ratio, the final crystalline phase first increases with a subsequent decrease followed by another increase and that the glass phase shows the opposite trend to that of the crystalline phase. Because

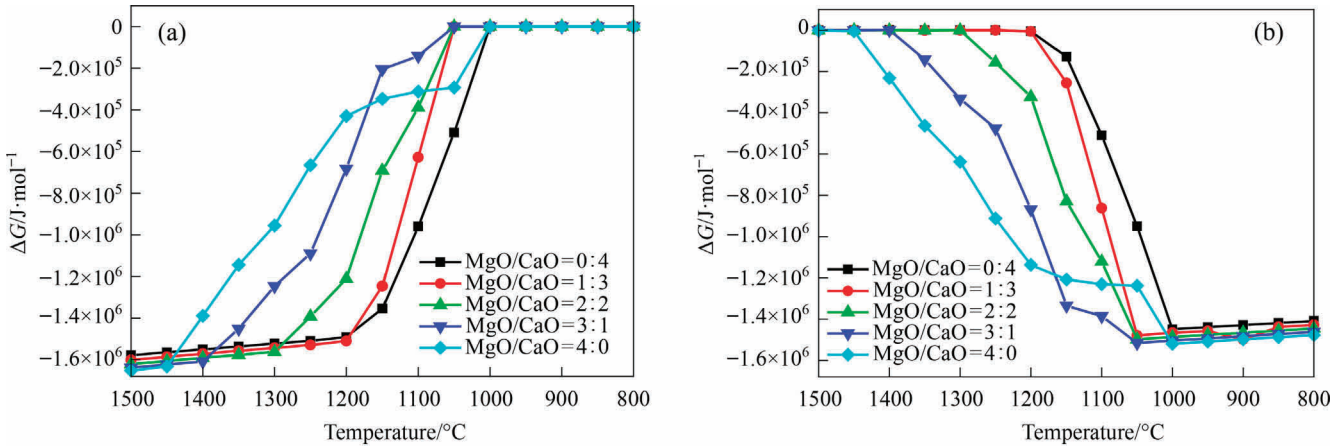

Fig. 3. ΔG of solid and liquid phases of the synthetic slags with different MgO/CaO ratios in the cooling process: (a) liquid phases; (b) solid phases.

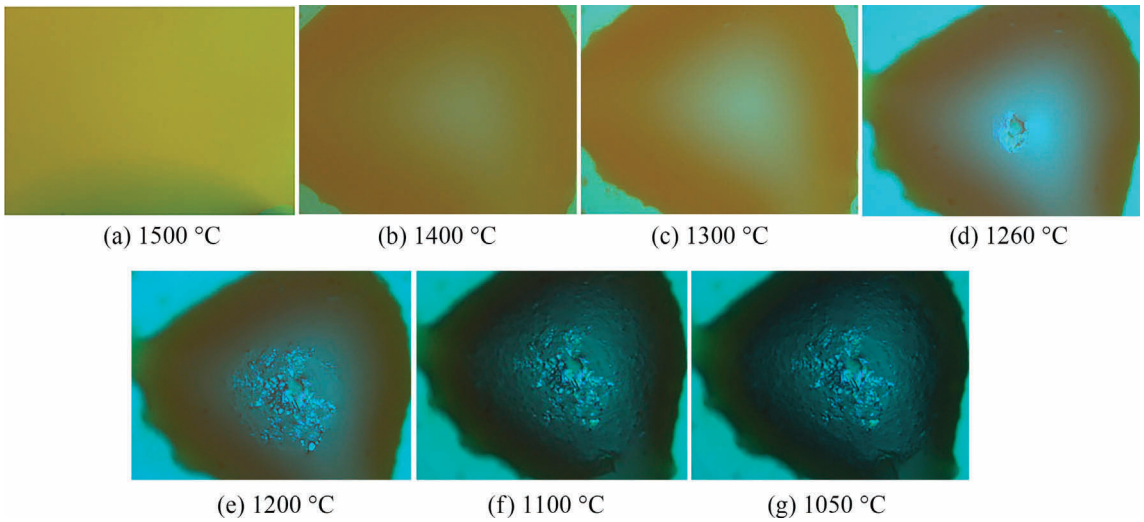

Fig. 4. Crystallization behaviour of the synthetic slags with 0:4 MgO/CaO ratio at a cooling rate of 10 °C·min^{-1}.

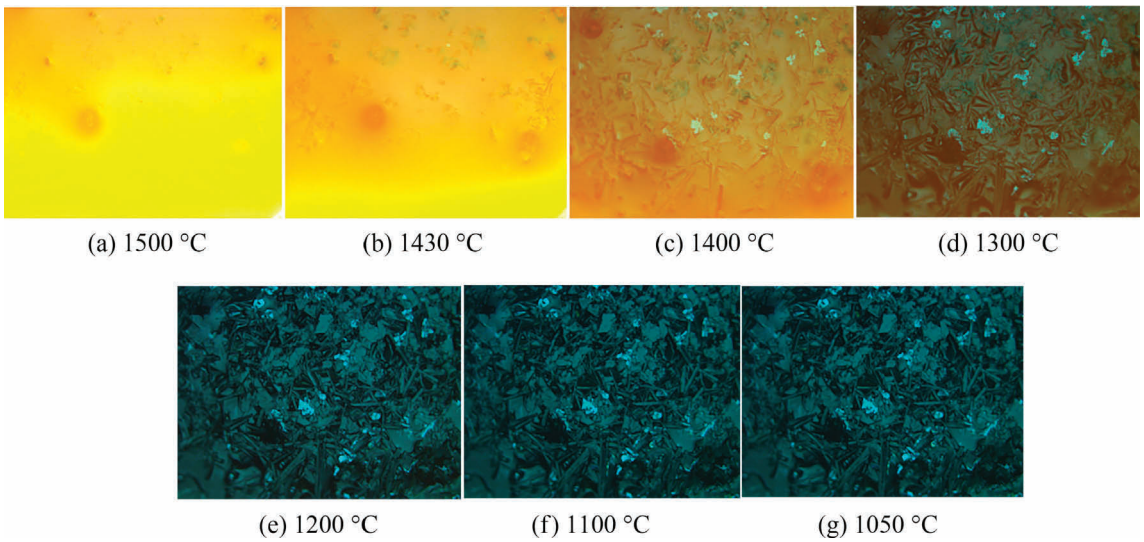

Fig. 5. Crystallization behaviour of the synthetic slags with 1:3 MgO/CaO ratios at a cooling rate of 10 °C·min^{-1}.

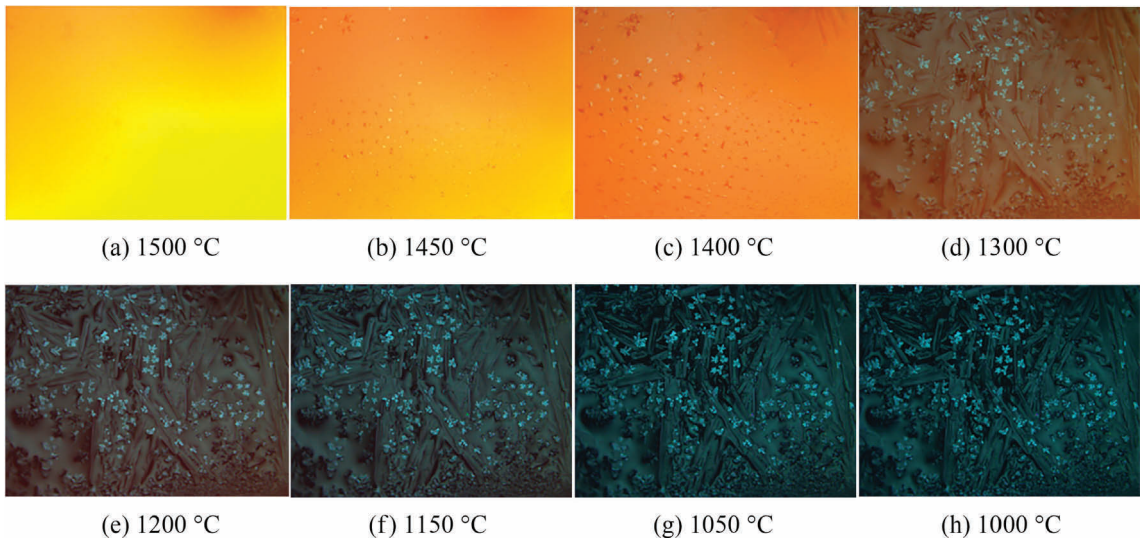

Fig. 6. Crystallization behaviour of the synthetic slags with 2:2 MgO/CaO ratio at a cooling rate of 10 °C·min^{-1}.

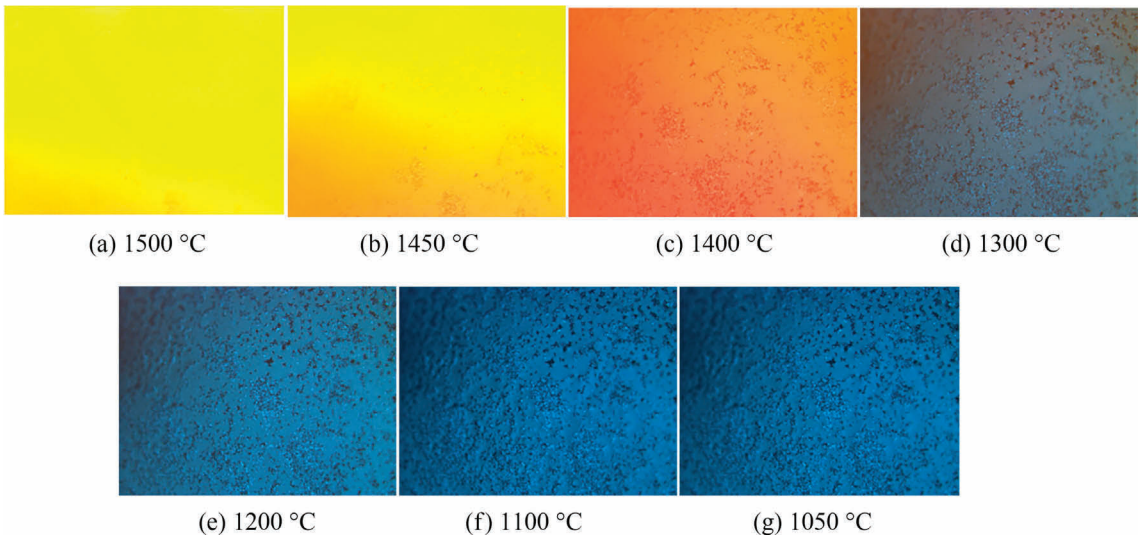

Fig. 7. Crystallization behaviour of the synthetic slags with 3:1 MgO/CaO ratio at a cooling rate of 10 °C·min^{-1}.

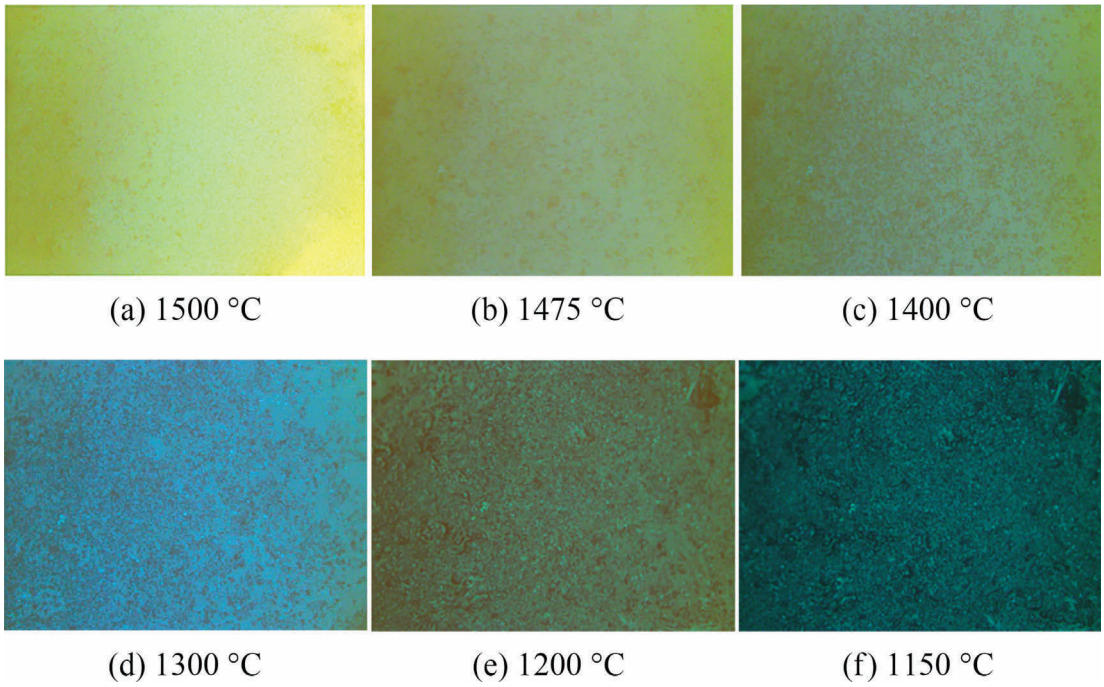

Fig. 8. Crystallization behaviour of the synthetic slags with 4:0 MgO/CaO ratio at a cooling rate of 10 °C·min^{-1}.

some of the samples have smaller size crystal in the crystallization process, the specific crystal shape cannot be observed under the magnification of HTSM. The phase distribution and morphology of the samples are further observed using SEM and EDS.

3.5. Crystal morphology analysis

Fig. 9 shows the results of crystal morphology and energy spectrum analysis of slag. To observe the crystalline shape and distribution vividly, some areas of the slag are amplified with different magnifications. Fig. 9(a), (a*), and (a-E) show that a small amount of strip and flake crystals containing Ca, Si, and Al are observed in the slag with a 0:4 MgO/CaO ratio, which is conjectured to be anorthite. These crystals are thin, and the crystalline outline is not clear enough, which is also consistent with the conclusion that the crystalline phase content is low. Fig. 9(b) and (b-E) show that when the MgO/CaO ratio is 1:3, many flake and strip crystals with large size containing mainly Ca, Si, and Al existing in the slag are conjectured to be anorthite. In addition, some rod-shaped crystals containing mainly Ca, Mg, Si, Al, and Fe are conjectured to be pyroxene. Fig. 9(c), (c*), (c**), (c-E), (c*-E), and (c**-E) show the characterization results of the slag with a 2:2 MgO/CaO ratio. Fig. 9(c) and (c-E) show that the columnar and long strip crystals with larger size in the slag are diopside and anorthite. However, the crystals in some areas are smaller, as shown in Fig. 9(c), and can not be clearly distinguished. These areas should be magnified in order to observe them. The characterization results after further magnification are presented in Fig. 9(c*), (c**), (c*-E), and (c**-E). As shown in Fig. 9(c*) and (c*-E), some crystals are stacked together with irregular granular, and part of the crystals are smooth strip with smaller

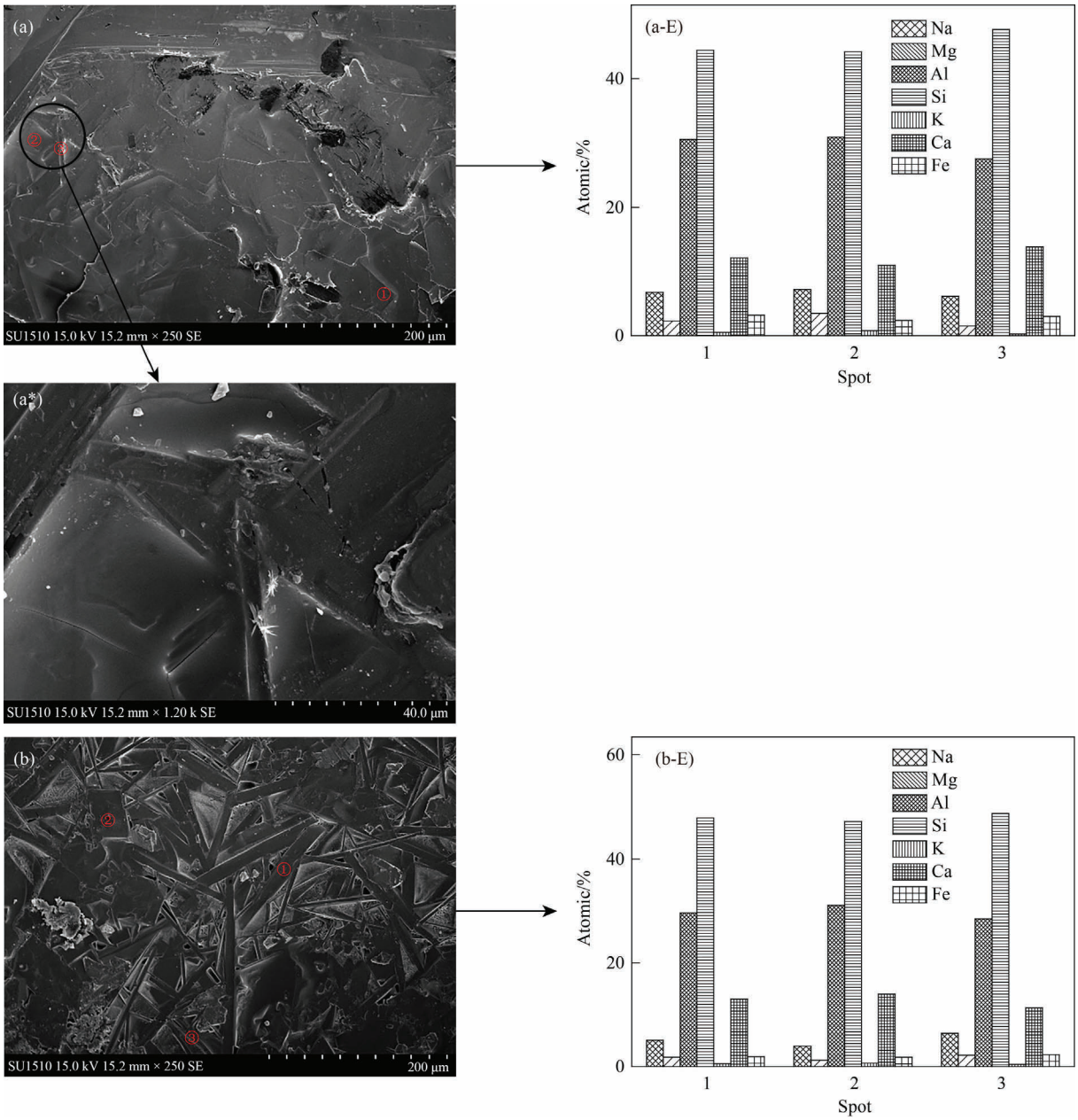

Fig. 9. SEM and EDS patterns of the synthetic slags withdifferent MgO/CaO ratios. (a), (a*), and (a-E): MgO/CaO = 0:4; (b) and (b-E): MgO/CaO = 1:3; (c), (c*), (c**), (c-E), (c*-E), and (c**-E): MgO/CaO = 2:2; (d), (d*), and (d-E): MgO/CaO = 3:1; (e), (e*), and (e-E): MgO/CaO = 4:0.

size. These crystals mainly contain Mg and Si in the slag, which are conjectured to be Mg-rich olivine. In addition, as shown in Fig. 9 (c*), (c**), (c*-E), and (c**-E), some polygonal crystals with smaller size mainly contain Mg and Al, conjectured to be Mg-rich spinel and most of these crystals are hexagonal and triangular crystals. The triangular crystal is also called a spiny crystal in some studies [33]. It can be inferred from the above analysis and from Fig. 6 of *in situ* observation that the smaller size crystalline phases are formed preferentially at higher temperatures is the Mg-bearing minerals, and thereafter the Ca-bearing minerals are formed with decreasing temperature. This corresponds with the FactSage results, as shown in Fig. 2(c), indicating that some Mg-bearing minerals are formed preferentially to Ca-bearing minerals at high temperature and that the formation of Ca-bearing minerals requires greater undercooling. In Fig. 9(d), some spiny crystals and some dense crystals appear in the slag with a 3:1 MgO/CaO ratio. The spiny crystals mainly contain Mg and Al, conjectured to be Mg-rich spinel. In Fig. 9(d*), most of the dense crystals in the slag with a 3:1 MgO/CaO ratio are observed upon magnification as small granular crystals with irregular accumulation and some spiny crystals. According to the analysis of the atomic ratio of a crystal phase, the dense crystals may be the Mg-rich spinel and Mg-rich olivine. Typical anorthite and diopside do not exist, and the atomic ratio of Ca was low in the energy spectrum analysis. Thus, it is inferred that the Ca-bearing mineral content is low, making its observation difficult. This may be because Al^{3+} and Si^{4+} participate preferentially in the formation of the Mg-rich spinel and Mg-rich olivine, which greatly reduce Al^{3+} and Si^{4+} and inhibit the formation of the Ca-bearing minerals. Mg^{2+} have a higher mobility due to the smaller radius of Mg^{2+} in comparison with Ca^{2+} [35,49,50]. Mg^{2+}, with its smaller radius, is favourable to the higher charge concentrations provided by the $\equiv SiO_2$ sites and

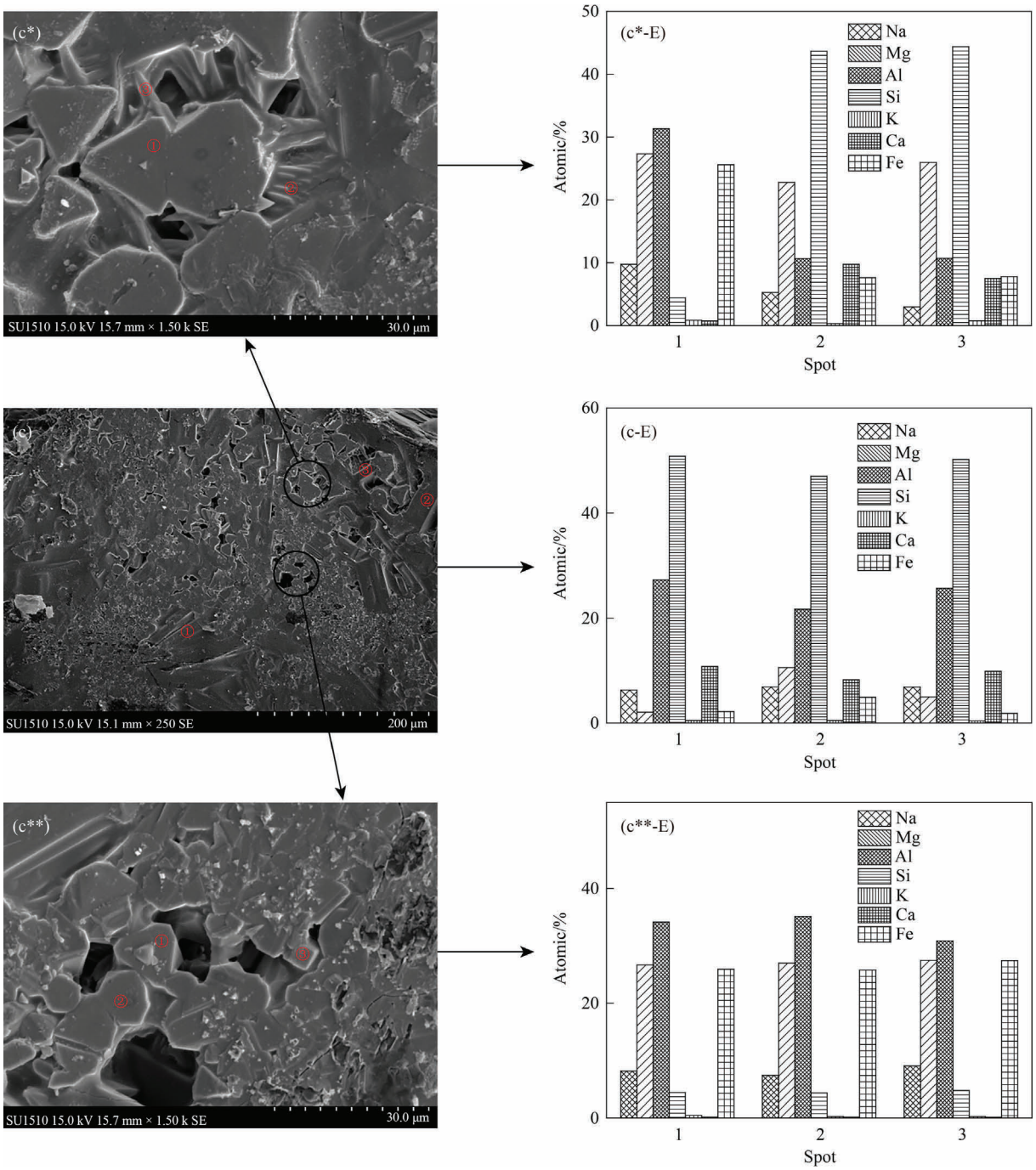

Fig. 9 (*continued*)

Ca^{2+} positions in the $\equiv SiO_2$ sites may be replaced by Mg^{2+} [51]. The previous literature shows that the shortening effect of MgO on binary glass is stronger than that of CaO, and the difference in the shortening effect is mainly attributed to the different binding strength of Mg and Ca with O [40]. The bond length of Mg—O is shorter than that of Ca—O, and its bond energy is greater than that of Ca—O, causing Mg and O to bond more closely than Ca and O [48,52,53]. In addition, Compare with Ca^{2+}, Mg^{2+} has a greater ionic field strength, a higher polarising power, and a stronger electrostatic interaction with surrounding ions [50,52,54,55]. Because of the high activity of Mg^{2+}, it is more easily attracted by nearby silicon/aluminum tetrahedron and react with it to generate a new Mg-bearing mineral, *e.g.* Mg-rich spinel or Mg-rich olivine [56]. Thus, the enhance tendency of MgO on crystallization is more effective than that of CaO. In addition, the Mg-rich spinel and Mg-rich olivine do not transform into diopside containing Ca and Mg. These cause the slag with a 3:1 MgO/CaO ratio to have a low final crystalline phase. The slag with a 4:0 MgO/CaO ratio has some olivine containing Mg and Si, existing in the form ofa long plate-like, as shown in Fig. 9(e). Some spinel and a small amount of olivine are closely and irregularly packed, as shown in Fig. 9(e*).

3.6. Viscosity–temperature characteristics analysis

The crystallization ratios of synthetic slags during cooling are obtained using ImageJ according to Figs. 4–8 photographed by

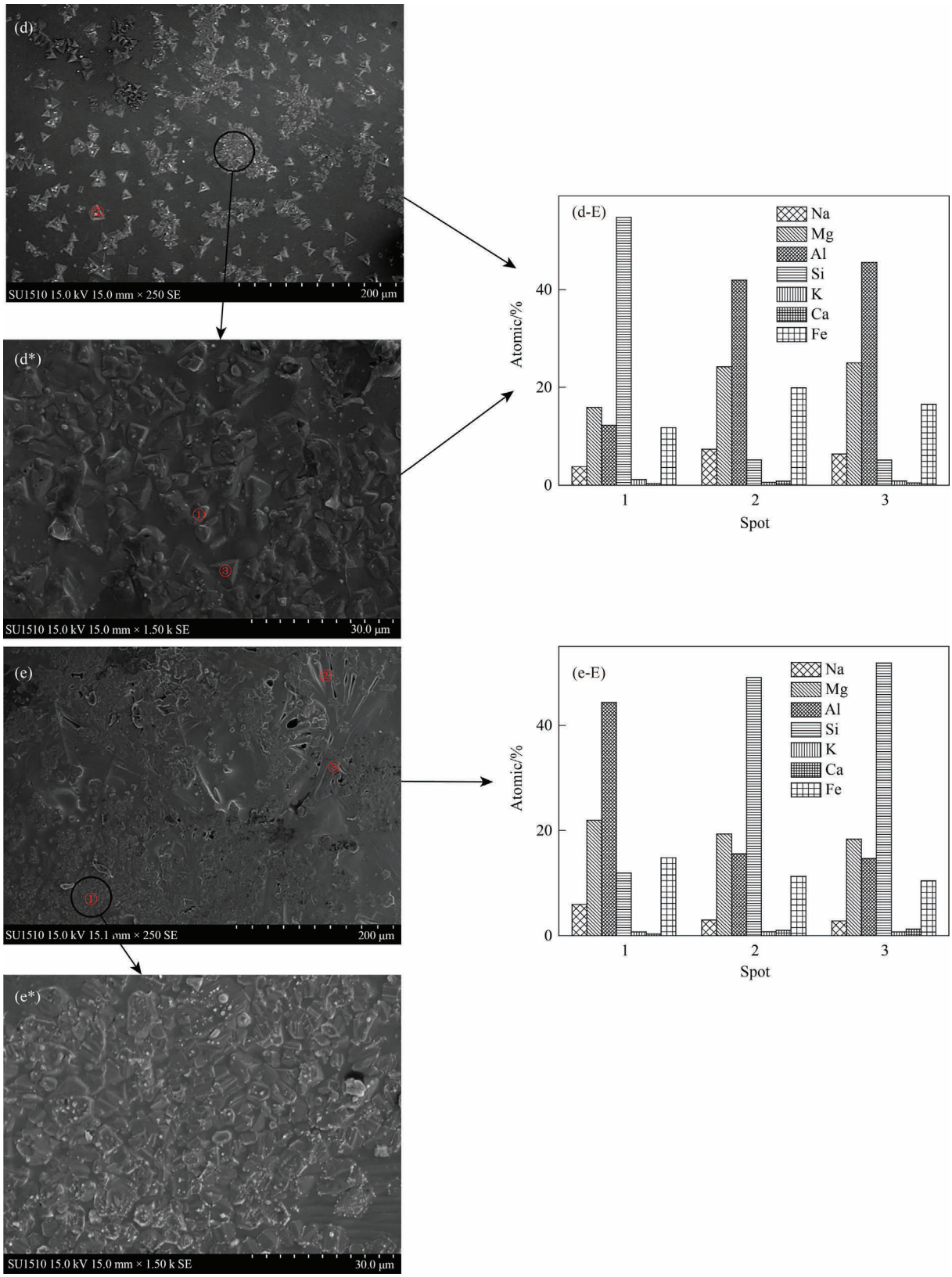

Fig. 9 (*continued*)

HTSM. Fig. 10 shows the changes in the crystallization ratios of synthetic slags with different MgO/CaO ratios in the cooling process. It is seen from Fig. 10 that the final crystallization contents of the synthetic slags with different MgO/CaO ratios differ, in that the final crystalline contents of the synthetic slags with MgO/CaO ratios of 1:3 and 4:0 are higher, and that of the synthetic slags with MgO/CaO ratios of 0:4, 2:2, and 3:1 were lower. During the cooling process, the crystallization ratios and rates of synthetic slags with

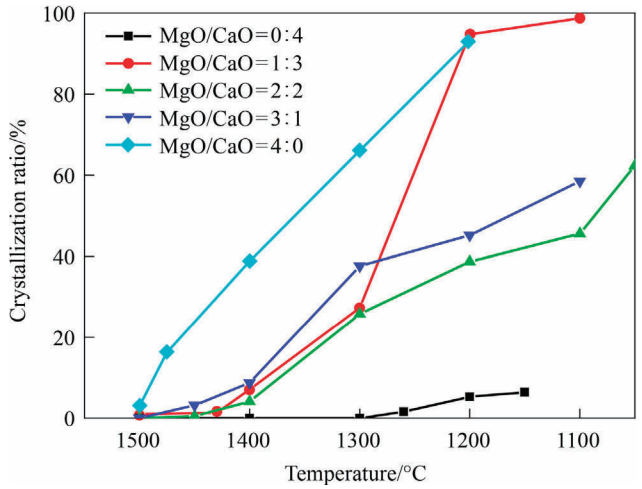

Fig. 10. Crystallization ratios of the synthetic slags with different MgO/CaO ratios in the cooling process.

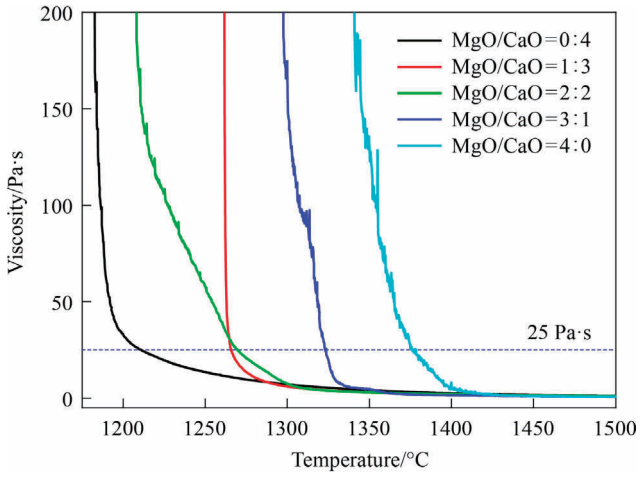

Fig. 11. Viscosity–temperature curves of the synthetic slags with different MgO/CaO ratios in the cooling process.

different MgO/CaO ratios also show different changing trends. When the MgO/CaO ratio is 0:4, the crystals begin to precipitate at lower temperatures and the crystallization rate is low. When the MgO/CaO ratio was 1:3, the crystallization ratio and rate are lower in the higher temperature range (1500–1300 °C). With decreasing temperature, the crystallization ratio increases greatly in the lower temperature range (1300–1200 °C). The increase in the crystalline content of synthetic slag within the lower temperature range is much higher than that in the higher temperature range. Together, Figs. 1, 2(b), and 3(b) infer that the addition of a small amount of MgO promotes the formation of diopside ($CaMgSi_2O_6$) in the lower temperature range. A large amount of anorthite and diopside are formed in the lower temperature range may have caused the significant increase in the crystallization ratio. When the MgO/CaO ratio is 2:2, the change in crystalline content is relatively gentle. When the temperature decline to 1300–1200 °C, the crystallization rate does not increase. Together, Figs. 1, 2(c), and 3(c) infer that in the lower temperature range, the decrease in anorthite and diopside formed leads to a lower crystallization ratio compared to that of the synthetic slag with a 1:3 MgO/CaO ratio. When the MgO/CaO ratio increase to 3:1 and 4:0, the crystallization ratios and rates are higher than that of the synthetic slags with MgO/CaO ratios of 0:4, 1:3, and 2:2 in the higher temperature range. This may be due to the formation of numerous Mg-rich crystalline phases in the synthetic slags with MgO/CaO ratios of 3:1 and 4:0 in the higher temperature range.

Fig. 11 shows the viscosity–temperature curves ofthe synthetic slags. The operating temperature range of an EFB gasifier requires the viscosity of the slag to be between 2–25 Pa·s. A high viscosity (viscosity > 25 Pa·s) leads to a difficulty in slag discharge, and a low viscosity (viscosity < 2 Pa·s) corrodes the refractory bricks in the gasifier. Table 2 shows the characteristic temperature parameters of the viscosity-temperature curves, where T_{p2} and T_{p25} are the temperatures corresponding to the viscosities of 2 and 25 Pa·s, respectively. T_{cv} is the critical viscosity temperature, and (T_{p2}–T_{p25}) is the effective slagging operating temperature range. As shown in Fig. 10, the synthetic slag with a 2:2 MgO/CaO ratio is plastic slag and has a smooth viscosity–temperature curve. The synthetic slag with 1:3 MgO/CaO ratio is, however, crystalline slag, and its viscosity shows a significant change near T_{cv}. The viscosity of the other three synthetic slags changes more gradually than that of the synthetic slag with a 1:3 MgO/CaO ratio but more dramatically than that of the synthetic slag with a 2:2 MgO/CaO ratio. As shown in Table 2, T_{p25} shows an increasing trend with the increase

Table 2
Relevant parameters of viscosity–temperature curves

Samples	T_{cv}/°C	T_{p2}/°C	T_{p25}/°C	T_{p2}–T_{p25}/°C
MgO/CaO (0:4)	1182	1427	1210	217
MgO/CaO (1:3)	1263	1389	1265	124
MgO/CaO (2:2)	1203	1394	1268	126
MgO/CaO (3:1)	1296	1370	1323	47
MgO/CaO (4:0)	1340	1421	1377	44

Note: T_{cv} = critical viscosity temperature.
T_{p2} = temperature at which the viscosity was 2 Pa·s.
T_{p25} = temperature at which the viscosity was 25 Pa·s.

in MgO/CaO ratio, indicating that the effective slagging operating temperature moves to the higher temperature range. However, the effective slagging operating temperature range of synthetic slags shows a decreasing trend, and the T_{cv} which first increases with a subsequent decrease followed by an increase. Of the five synthetic slags, the one with a MgO/CaO ratio of 0:4 is relatively suitable for slag discharge in an EFB gasifier becausethe effective slagging operating temperature range is the widest (217 °C) and T_{p25} was the lowest (1210 °C). The synthetic slags with 2:2 and 1:3 MgO/CaO ratios show a similar effective slagging operating temperature range, T_{p2} and T_{p25} (effective slagging operating temperature range: 124 and 126 °C; T_{p2}: 1389 and 1394 °C; T_{p25}: 1265 and 1268 °C). However, because the synthetic slag with a 1:3 MgO/CaO ratio was a crystalline slag, the actual slagging operating temperature should be much higher than T_{cv}, to avoid a sudden increase in crystallization which can potentially lead to a rapid increase in viscosity. Therefore, the actual slagging operating temperature range is much lower than 124 °C. The synthetic slag with a 2:2 MgO/CaO ratio is a plastic slag, and its viscosity changes gently near T_{p25}: thus, the synthetic slag for EFB gasification would have a better operational flexibility. For the synthetic slags with 3:1 and 4:0 MgO/CaO ratios, the effective slagging operating temperature ranges are narrow (47 and 44 °C, respectively), and the actual slagging operating temperatures are in the higher temperature range. This may cause a large viscosity change due to unstable temperatures in an EFB gasifier, resulting in difficult slag discharge.

In industrial coal blending and gasification operations, the base/acid ratio of slag is an important parameter affecting the slag discharge characteristics [57]. However, when the base/acid ratio is constant, the change in MgO/CaO ratios will also cause the slag to show different slag discharge characteristics. The above analysis

infers that with an increase in the MgO/CaO ratio, the main temperature range of crystallization moves to the higher temperature range and that the T_{p25} also increases. The crystalline ratios and rates ofthe synthetic slags with MgO/CaO ratios of 0:4, 1:3, and 2:2 are lower than that of the synthetic slags with 3:1 and 4:0 MgO/CaO ratios at higher temperatures, which may be the reason for the lower T_{p25} of these three slags compared to the synthetic slags with MgO/CaO ratios of 3:1 and 4:0. In addition, the different types of crystalline phases will affect the viscosity. In the synthetic slag with a 1:3 MgO/CaO ratio, the anorthite easily moves irregularly inside the slag at higher temperatures due to its low viscosity, low crystalline content, and thin crystals [58]. This causes a slow viscosity change in the higher temperature range of the synthetic slag. As the temperature decrease, numerous diopside containing Mg and Ca and anorthite are formed in the lower temperature range, resulting in a sharp increase in viscosity. The anorthite and diopside contents are lower in the synthetic slag with a 2:2 MgO/CaO ratio than those with a 1:3 MgO/CaO ratio in the lower temperature range. The increase in crystalline content is relatively gentle in the synthetic slag with a 2:2 MgO/CaO ratio, resulting in a smooth viscosity change, which is more suitable for slag discharge in an EFB gasifier. Although the final crystallization content of the synthetic slag with a 3:1 MgO/CaO ratio was lower than that of thesynthetic slags with MgO/CaO ratios of 1:3, 2:2, and 4:0, many Mg-rich crystalline phases are formed at higher temperatures and most of them are linked like network which may cause a higher T_{p25} (1323 °C) [59]. The crystallization rate and ratio of the synthetic slag with a 4:0 MgO/CaO ratio are the highest in the higher temperature range, which potentially led to the highest T_{p25} (1377 °C).

4. Conclusions

The crystallization characteristics and fluidity of five synthetic slags with different MgO/CaO ratios were studied. The final crystalline phase compositions of the slags were obtained using the water quenching method and XRD. The theoretical mineral composition changes and ΔG of the solid and liquid phases during the cooling process were calculated using FactSage. The surface morphology change and the crystallization ratio in the crystalline phase during the cooling process was observed using HSTM, ImageJ, and SEM-EDS, and the viscosity was obtained using a high temperature rotational viscometer. The results are as follows:

(1) The synthetic slags with different MgO/CaO ratios show different crystallization behaviours, affecting their fluidity. With an increase in the MgO/CaO ratio, the initial crystallization temperature increases perceptibly. The final crystalline content shows an increasing trend initially, a decreasing trend subsequently, and another increasing trend finally.

(2) T_{p25} is the lowest for the synthetic slag with a 0:4 MgO/CaO ratio, and it has a significantly wide slagging operating temperature range. When the MgO/CaO ratio was 2:2, the synthetic slag shows a gentle crystallization ratio change in the lower temperature range, resulting in a mild viscosity–temperature curve. These two slags are more suitable for slag discharge of an EFB gasifier. The rapid increase of diopside and anorthite in the lower temperature range leads to a sharp viscosity change in the synthetic slags with a 1:3 MgO/CaO ratio. The large amount of Mg-rich crystalline phase formation in the higher temperature range lead to high T_{p25} and narrow slagging operating temperature ranges of the synthetic slags with 3:1 and 4:0 MgO/CaO ratios. These may guide the slag discharge of Zhundong coal.

(3) Both Ca^{2+} and Mg^{2+} are network modifiers to destroy the network structure; however, the promoting effect of MgO on slag crystallization is more obvious than that of CaO. Compared with Ca^{2+}, Mg^{2+} can more easily participate in the reaction at higher temperature and react with the surrounding silicon/aluminum tetrahedron to form new minerals. Thus, Mg-rich spinel and Mg-rich olivine are formed preferentially to Ca-bearing minerals of the slag with the same addition of MgO and CaO with decreasing temperature. In addition, the amount of crystalline phase containing Mg and Ca is formed in the lower temperature rangeis closely related to the MgO/CaO ratio.

Data Availability

Data will be made available on request.

Declaration of Competing Interest

The authors declare that they have no known competing financial interests or personal relationships that could have appeared to influence the work reported in this paper.

Acknowledgements

This research was financially supported by the National Natural Science Foundation of China (21878082).

References

[1] Y.F. Shen, Y.F. Hu, M.J. Wang, W.R. Bao, L.P. Chang, K.C. Xie, Speciation and thermal transformation of sulfur forms in high-sulfur coal and its utilization in coal-blending coking process: A review, *Chin. J. Chem. Eng.* 35 (2021) 70–82.
[2] W.J. Shi, L.X. Kong, J. Bai, J. Xu, W.C. Li, Z.Q. Bai, W. Li, Effect of CaO/Fe_2O_3 on fusion behaviors of coal ash at high temperatures, *Fuel Process. Technol.* 181 (2018) 18–24.
[3] K.C. Xie, Reviews of clean coal conversion technology in China: Situations & challenges, *Chin. J. Chem. Eng.* 35 (2021) 62–69.
[4] Z.J. Shen, H. Nikolic, L.S. Caudill, K.L. Liu, A deep insight on the coal ash-to-slag transformation behavior during the entrained flow gasification process, *Fuel* 289 (2021) 119953.
[5] X.D. Liu, Z.W. Jin, Y.H. Jing, P.P. Fan, Z.L. Qi, W.R. Bao, J.C. Wang, X.H. Yan, P. Lv, L.P. Dong, Review of the characteristics and graded utilisation of coal gasification slag, *Chin. J. Chem. Eng.* 35 (2021) 92–106.
[6] H.L. Fan, F.H. Li, Q.Q. Guo, M.X. Guo, Effect of high silicon-aluminum coal ashes on sintering and fusion characteristics of a potassium-rich biomass ash, *J. Energy Inst.* 93 (5) (2020) 1781–1789.
[7] C.B. Nguyen, J. Scherer, M. Hartwich, A. Richter, The morphology evolution of char particles during conversion processes, *Combust. Flame* 226 (2021) 117–128.
[8] F.H. Guo, X. Zhao, Y. Guo, Y.X. Zhang, J.J. Wu, Fractal analysis and pore structure of gasification fine slag and its flotation residual carbon, *Colloids Surf. A Physicochem. Eng. Aspects* 585 (2020) 124148.
[9] Y. Li, F.H. Li, M.J. Ma, B. Yu, C.Y. Zhao, Y.T. Fang, Prediction of ash flow temperature based on liquid phase mass fraction by FactSage, *J. Energy Inst.* 93 (6) (2020) 2228–2231.
[10] L.C. Xie, Y. Lv, L. Xu, The influence of the high potassium biomass on the ash fusion characteristics of coal, *J. Energy Inst.* 95 (2021) 52–60.
[11] G.X. Wu, E. Yazhenskikh, K. Hack, M. Müller, Viscosity model for oxide melts relevant to fuel slags. Part 2: The system SiO_2–Al_2O_3–CaO–MgO–Na_2O–K_2O, *Fuel Process. Technol.* 138 (2015) 520–533.
[12] L.M. Zhang, J.F. Wang, X.D. Song, Y.H. Bai, M. Yao, G.S. Yu, Influence of biomass ash additive on fusion characteristics of high-silicon-aluminum coal ash, *Fuel* 282 (2020) 118876.
[13] Q.H. Guo, Z.J. Zhou, F.C. Wang, G.S. Yu, Slag properties of blending coal in an industrial OMB coal water slurry entrained-flow gasifier, *Energy Convers. Manag.* 86 (2014) 683–688.
[14] Z.Y. Zhang, S.S. Pang, T. Levi, Influence of AAEM species in coal and biomass on steam co-gasification of chars of blended coal and biomass, *Renew. Energy* 101 (2017) 356–363.
[15] M. Li, F.H. Li, Q.R. Liu, Y.T. Fang, H.X. Xiao, Regulation of ash fusibility for high ash-fusion-temperature (AFT) coal by industrial sludge addition, *Fuel* 244 (2019) 91–103.
[16] X. Dai, J. Bai, P. Yuan, S.Y. Du, D.T. Li, X.D. Wen, W. Li, The application of molecular simulation in ash chemistry of coal, *Chin. J. Chem. Eng.* 28 (11) (2020) 2723–2732.

[17] S. Park, I.S. Ye, J. Oh, C. Ryu, J.H. Koo, Gas and particle flow characteristics in the gas reversing chamber of a syngas cooler for a 300 MWe IGCC process, *Appl. Therm. Eng.* 70 (1) (2014) 388–396.

[18] L.X. Kong, J. Bai, W. Li, Viscosity-temperature property of coal ash slag at the condition of entrained flow gasification: A review, *Fuel Process. Technol.* 215 (2021) 106751.

[19] W.W. Xuan, K.J. Whitty, Q.L. Guan, D.P. Bi, Z.H. Zhan, J.S. Zhang, Influence of SiO_2/Al_2O_3 on crystallization characteristics of synthetic coal slags, *Fuel* 144 (2015) 103–110.

[20] W.W. Xuan, H.N. Wang, D.H. Xia, Depolymerization mechanism of CaO on network structure of synthetic coal slags, *Fuel Process. Technol.* 187 (2019) 21–27.

[21] X. Liu, G.S. Yu, J.L. Xu, Q.F. Liang, H.F. Liu, Viscosity fluctuation behaviors of coal ash slags with high content of calcium and low content of silicon, *Fuel Process. Technol.* 158 (2017) 115–122.

[22] W.J. Shi, M. Laabs, M. Reinmöller, J. Bai, S. Guhl, L.X. Kong, H.Z. Li, B. Meyer, W. Li, *In-situ* analysis of the effect of CaO/Fe_2O_3 addition on ash melting and sintering behavior for slagging-type applications, *Fuel* 285 (2021) 119090.

[23] F. Wang, M. Yao, H.Y. Kan, J.P. Kuang, P. Li, J.S. Zhang, Y.X. Zhang, Effect of Al_2O_3/CaO on the melting and mineral transformation of Ningdong coal ash, *Chin. J. Chem. Eng.* 28 (12) (2020) 3110–3116.

[24] Y.Q. Niu, Y.H. Gong, X. Zhang, Y. Liang, D.H. Wang, S.E. Hui, Effects of leaching and additives on the ash fusion characteristics of high-Na/Ca Zhundong coal, *J. Energy Inst.* 92 (4) (2019) 1115–1122.

[25] Y. Bottinga, D.F. Weill, The viscosity of magmatic silicate liquids; A model calculation, *Am. J. Sci.* 272 (5) (1972) 438–475.

[26] Q.Q. Ren, Y.Z. Zhang, Y. Long, Z.S. Zou, S.S. Chen, J. Li, Investigation on the effect of MgO content on the crystallization behavior of synthetic BF slag, *Mater. Manuf. Process.* 33 (15) (2018) 1654–1660.

[27] H.P. Yuan, Q.F. Liang, X. Gong, Crystallization of coal ash slags at high temperatures and effects on the viscosity, *Energy Fuels* 26 (6) (2012) 3717–3722.

[28] W.W. Xuan, J.S. Zhang, D.H. Xia, Crystallization characteristics prediction of coal slags based on SiO_2–Al_2O_3–CaO–Fe_2O_3–MgO components, *J. Ind. Eng. Chem.* 59 (2018) 341–349.

[29] J. Yang, J.Q. Zhang, Y. Sasaki, O. Ostrovski, C. Zhang, D.X. Cai, Y. Kashiwaya, *In-situ* study of crystallisation behaviour of CaO–SiO_2–Na_2O–B_2O_3–TiO_2–Al_2O_3–MgO–Li_2O fluorine-free mould fluxes with different CaO/SiO_2 ratios, *ISIJ Int.* 56 (4) (2016) 574–583.

[30] Z.H. Yang, Q. Lin, S.C. Lu, Y. He, G.D. Liao, Y. Ke, Effect of CaO/SiO_2 ratio on the preparation and crystallization of glass-ceramics from copper slag, *Ceram. Int.* 40 (5) (2014) 7297–7305.

[31] S.F. Zhang, X. Zhang, W. Liu, X.W. Lv, C.G. Bai, L. Wang, Relationship between structure and viscosity of CaO–SiO_2–Al_2O_3–MgO–TiO_2 slag, *J. Non Cryst. Solids* 402 (2014) 214–222.

[32] L.X. Kong, J. Bai, H.Z. Li, X.D. Chen, J. Wang, Z.Q. Bai, Z.X. Guo, W. Li, The mineral evolution during coal washing and its effect on ash fusion characteristics of Shanxi high ash coals, *Fuel* 212 (2018) 268–273.

[33] W.W. Xuan, J.S. Zhang, D.H. Xia, The influence of MgO on the crystallization characteristics of synthetic coal slags, *Fuel* 222 (2018) 523–528.

[34] K. Dimitriadis, D.U. Tulyaganov, K.C. Vasilopoulos, M.A. Karakassides, S. Agathopoulos, Influence of K and Mg substitutions on the synthesis and the properties of CaO–MgO–SiO_2/Na_2O, P_2O_5, CaF_2 bioactive glasses, *J. Non Cryst. Solids* 573 (2021) 121140.

[35] J. Massera, L. Hupa, M. Hupa, Influence of the partial substitution of CaO with MgO on the thermal properties and *in vitro* reactivity of the bioactive glass S53P4, *J. Non Cryst. Solids* 358 (18–19) (2012) 2701–2707.

[36] X.M. Li, L.F. Zhi, W.J. Shi, L.X. Kong, J. Bai, J.L. Yu, M. Reinmöller, S. Guhl, B. Meyer, W. Li, Effect of K_2O/Na_2O on fusion behavior of coal ash with high silicon and aluminum level, *Fuel* 265 (2020) 116964.

[37] C.L. Wu, B.B. Wang, J.Q. Zheng, H.X. Li, Flux mechanism of compound flux on ash and slag of coal with high ash melting temperature, *Chin. J. Chem. Eng.* 27 (5) (2019) 1200–1206.

[38] C.L. Wu, Y. Xin, X. Liu, H.X. Li, F.C. Jiao, Synergistic effect of CaO and MgO addition on coal ash fusibility in a reducing atmosphere, *Asia Pac. J. Chem. Eng.* 14 (4) (2019) e2324.

[39] C.H. Jiang, K.J. Li, J.L. Zhang, Z.J. Liu, L.L. Niu, W. Liang, M.M. Sun, H.B. Ma, Z.M. Wang, The effect of CaO and MgO on the structure and properties of coal ash in the blast furnace: A molecular dynamics simulation and thermodynamic calculation, *Chem. Eng. Sci.* 210 (2019) 115226.

[40] S. Vargas, F.J. Frandsen, K. Dam-Johansen, Rheological properties of high-temperature melts of coal ashes and other silicates, *Prog. Energy Combust. Sci.* 27 (3) (2001) 237–429.

[41] C.W. Bale, E. Bélisle, P. Chartrand, S.A. Decterov, G. Eriksson, A.E. Gheribi, K. Hack, I.H. Jung, Y.B. Kang, J. Melançon, A.D. Pelton, S. Petersen, C. Robelin, J. Sangster, P. Spencer, M.A. van Ende, Reprint of: FactSage thermochemical software and databases, 2010–2016, *Calphad* 55 (2016) 1–19.

[42] C.W. Bale, P. Chartrand, S.A. Degterov, G. Eriksson, K. Hack, R.B. Mahfoud, J. Melançon, A.D. Pelton, S. Petersen, FactSage thermochemical software and databases, *Calphad* 26 (2) (2002) 189–228.

[43] Z.J. Shen, J. Zhou, X. Liu, Q.F. Liang, H.F. Liu, A deep insight on the correlation between slag viscosity fluctuation and decomposition of sulfur-bearing minerals in the entrained flow gasifier, *Energy* 196 (2020) 117049.

[44] M. Liu, Z.J. Shen, Q.F. Liang, J.L. Xu, H.F. Liu, *In situ* experimental study of CO_2 gasification of petcoke particles on molten slag surface at high temperature, *Fuel* 285 (2021) 119158.

[45] X. Dai, J. Bai, D.T. Li, P. Yuan, T.G. Yan, L.X. Kong, W. Li, Experimental and theoretical investigation on relationship between structures of coal ash and its fusibility for Al_2O_3–SiO_2–CaO–FeO system, *J. Fuel Chem. Technol.* 47 (6) (2019) 641–648.

[46] I. Sunagawa, *In situ* investigation of nucleation, growth, and dissolution of silicate crystals at high temperatures, *Annu. Rev. Earth Planet. Sci.* 20 (1992) 113–142.

[47] Y.S. Ma, G.X. Wu, Q.H. Guo, X. Liu, Y. Gong, G.S. Yu, Investigation of fluctuation behavior in viscosity of coal slags used in entrained-flow gasifiers, *Fuel Process. Technol.* 181 (2018) 133–141.

[48] X. Dai, J. Bai, Q. Huang, Z. Liu, X.J. Bai, C.T. Lin, W. Li, W.P. Guo, X.D. Wen, S.Y. Du, Coal ash fusion properties from molecular dynamics simulation: the role of calcium oxide, *Fuel* 216 (2018) 760–767.

[49] K. Gong, C.E. White, Predicting CaO–(MgO) –Al_2O_3–SiO_2 glass reactivity in alkaline environments from force field molecular dynamics simulations, *Cem. Concr. Res.* 150 (2021) 106588.

[50] Y.M. Gao, S.B. Wang, C. Hong, X.J. Ma, F. Yang, Effects of basicity and MgO content on the viscosity of the SiO_2–CaO–MgO–9wt%Al_2O_3 slag system, *Int. J. Miner. Metall. Mater.* 21 (4) (2014) 353–362.

[51] F.J. Pei, H.W. Guo, P. Li, B.J. Yan, J. Li, P. Yang, G.H. Zhu, Influence of low magnesia content on the CaO–Al_2O_3–SiO_2 glass-ceramics: Its crystallization behaviour, microstructure and physical properties, *Ceram. Int.* 44 (16) (2018) 20132–20139.

[52] H.C. Li, D.G. Wang, J.H. Hu, C.Z. Chen, Effect of the partial substitution of K_2O, MgO, B_2O_3 for CaO on crystallization, structure and properties of Na_2O–CaO–SiO_2–P_2O_5 system glass-ceramics, *Mater. Lett.* 106 (2013) 373–376.

[53] J. Ma, C.Z. Chen, D.G. Wang, Y. Jiao, J.Z. Shi, Effect of magnesia on the degradability and bioactivity of sol–gel derived SiO_2–CaO–MgO–P_2O_5 system glasses, *Colloids Surf. B Biointerfaces* 81 (1) (2010) 87–95.

[54] S.J. Watts, R.G. Hill, M.D. O'Donnell, R.V. Law, Influence of magnesia on the structure and properties of bioactive glasses, *J. Non Cryst. Solids* 356 (9–10) (2010) 517–524.

[55] J. Ma, C.Z. Chen, D.G. Wang, J.H. Hu, Effect of magnesia on structure, degradability and *in vitro* bioactivity of CaO–MgO–P_2O_5–SiO_2 system ceramics, *Mater. Lett.* 65 (1) (2011) 130–133.

[56] M.W. Liu, J.B. Guo, Y.T. Shao, Effects of CaO and MgO contents on the properties of lightweight aggregate produced from municipal solid wastes, *Constr. Build. Mater.* 259 (2020) 120398.

[57] W.J. Shi, J. Bai, L.X. Kong, H.Z. Li, Z.Q. Bai, S.V. Vassilev, W. Li, An overview of the coal ash transition process from solid to slag, *Fuel* 287 (2021) 119537.

[58] W.W. Xuan, H.N. Wang, D.H. Xia, *In-situ* observation of crystallization inside coal slags and influence of crystals on flow behavior, *Fuel* 251 (2019) 242–248.

[59] W.W. Xuan, J.S. Zhang, D.H. Xia, Crystallization characteristics of a coal slag and influence of crystals on the sharp increase of viscosity, *Fuel* 176 (2016) 102–109.